

## Memory effects in nanoparticle dynamics and transport

Tarun Sanghi, Ravi Bhaduria, and N. R. Aluru

Citation: *The Journal of Chemical Physics* **145**, 134108 (2016); doi: 10.1063/1.4964287

View online: <http://dx.doi.org/10.1063/1.4964287>

View Table of Contents: <http://scitation.aip.org/content/aip/journal/jcp/145/13?ver=pdfcov>

Published by the AIP Publishing

---

### Articles you may be interested in

[Effects of ferroelectric nanoparticles on ion transport in a liquid crystal](#)

*Appl. Phys. Lett.* **105**, 151905 (2014); 10.1063/1.4898581

[Nanoparticle size effect on the magnetic and transport properties of \(La<sub>0.7</sub>Sr<sub>0.3</sub>\)<sub>0.9</sub>Mn<sub>1.1</sub>O<sub>3</sub> manganites](#)

*Low Temp. Phys.* **35**, 568 (2009); 10.1063/1.3170933

[Charge transfer effect in the polyaniline-gold nanoparticle memory system](#)

*Appl. Phys. Lett.* **90**, 053101 (2007); 10.1063/1.2434167

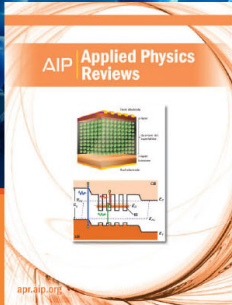
[Noncontinuum effects in nanoparticle dynamics in polymers](#)

*J. Chem. Phys.* **124**, 221102 (2006); 10.1063/1.2209241

[Memory effects and magnetic interactions in a  \$\gamma\$ -Fe<sub>2</sub>O<sub>3</sub> nanoparticle system](#)

*J. Appl. Phys.* **97**, 10J507 (2005); 10.1063/1.1853898

---



**NEW Special Topic Sections**

**NOW ONLINE**  
Lithium Niobate Properties and Applications:  
Reviews of Emerging Trends

**AIP** | Applied Physics  
Reviews

# Memory effects in nanoparticle dynamics and transport

Tarun Sanghi, Ravi Bhaduria, and N. R. Aluru<sup>a)</sup>

Department of Mechanical Science and Engineering, Beckman Institute for Advanced Science and Technology, University of Illinois at Urbana-Champaign, Urbana, Illinois 61801, USA

(Received 26 June 2016; accepted 21 September 2016; published online 7 October 2016)

In this work, we use the generalized Langevin equation (GLE) to characterize and understand memory effects in nanoparticle dynamics and transport. Using the GLE formulation, we compute the memory function and investigate its scaling with the mass, shape, and size of the nanoparticle. It is observed that changing the mass of the nanoparticle leads to a rescaling of the memory function with the reduced mass of the system. Further, we show that for different mass nanoparticles it is the initial value of the memory function and not its relaxation time that determines the “memory” or “memoryless” dynamics. The size and the shape of the nanoparticle are found to influence both the functional-form and the initial value of the memory function. For a fixed mass nanoparticle, increasing its size enhances the memory effects. Using GLE simulations we also investigate and highlight the role of memory in nanoparticle dynamics and transport. *Published by AIP Publishing.* [<http://dx.doi.org/10.1063/1.4964287>]

## I. INTRODUCTION

Understanding the dynamics and transport of natural and engineered nanoparticles in a host fluid environment is necessary for various nanofluidic applications. Nanoparticles lie at the boundary between the macroscopic and atomistic regimes and multiscale techniques are required to understand their behavior. In this work, we use the generalized Langevin equation (GLE) formulation to understand memory effects in nanoparticle diffusion and transport. The description of a nanoparticle’s motion by a GLE provides a powerful coarse-grained multi-scale approach to simulate its dynamics and transport in a host fluid environment. With the advent of nanobiotechnology, there has been a growing interest in using GLE based stochastic simulations as a viable alternative to (a) investigate the so-called rare events whose timescales are still out of reach of conventional molecular dynamics (MD) simulation and (b) efficiently simulate processes such as self-assembly or agglomeration of nanoparticles in a solvent/host environment, which become computationally very expensive in MD simulations because of explicit atomistic treatment of the solvent/host environment molecules.<sup>1–3</sup> GLE describes the influence of the host fluid on the dynamics of the nanoparticle in terms of two counteracting forces: a projected or random force that the host fluid exerts on the nanoparticle and a dissipative force that describes the response of the host fluid to the dynamics of the nanoparticle. The dissipative force is characterized by a time dependent memory function; and memory function and projected force are related through the fluctuation-dissipation theorem.<sup>4,5</sup> On the basis of GLE formulation, we extract the memory function and investigate its scaling with the mass, size, and shape of the nanoparticle. The systems we investigate are fullerene based nanoparticles (see Fig. 1) immersed in water. Fullerenes are among the most

widely studied nanoparticles owing to their potential uses in electronics, photonics, and medical applications.<sup>6–9</sup>

The remainder of the paper is organized as follows: In Sec. II, we first review the GLE formulation to describe the dynamics of a nanoparticle in a host fluid. We also discuss how the equipartition theorem is modified in MD ensembles of unequal mass particles with periodic boundary conditions (PBCs). This knowledge is needed to correctly analyze the MD simulation results of a heavier mass nanoparticle immersed in the lighter mass host fluid. MD simulation details and numerical procedure used to perform GLE simulations are provided in Sec. III. In Sec. IV, we first discuss the scaling of memory with the mass of the nanoparticle. Then we study its scaling with the size and the shape of the nanoparticle. We also discuss GLE simulation based examples to investigate and highlight the role of memory in nanoparticle dynamics and transport. Finally, conclusions are presented in Sec. V.

## II. GLE FORMULATION AND MEMORY EFFECTS

The description of a particle’s motion by a GLE provides a powerful coarse-grained multiscale approach to study its equilibrium correlation functions and relaxation in the host fluid environment. Using Mori-Zwanzig projector operator techniques, the Hamilton’s equation of motion for a nanoparticle (solute) of mass  $M$  interacting with  $N$  particles of mass  $m$  (host fluid/solvent) can be written in the mathematically equivalent form as<sup>4,5</sup>

$$M\dot{V}(t) = -M \int_0^t K(t-t')V(t')dt' + R(t), \quad (1a)$$

$$\dot{X}(t) = V(t). \quad (1b)$$

Here  $X$  and  $V$  are, respectively, the position and the velocity,  $K(t)$  is the memory function, and  $R(t)$  is a “projected or random” force with statistical properties<sup>4,5</sup>

<sup>a)</sup>Electronic mail: aluru@illinois.edu

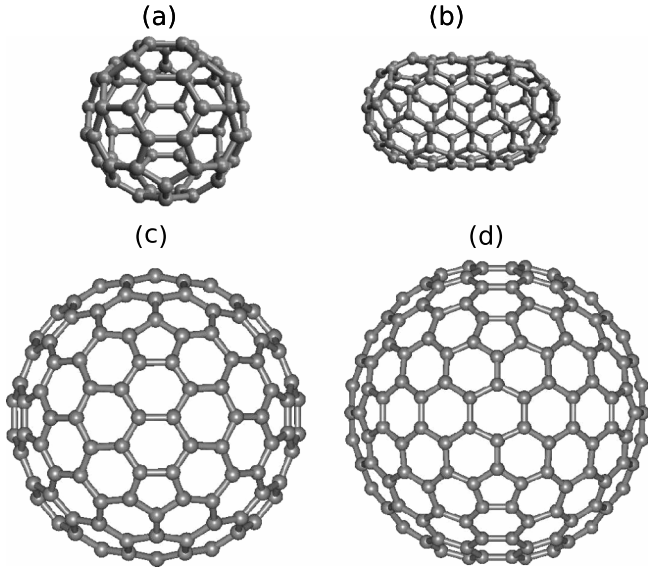


FIG. 1. Fullerene nanoparticles studied: (a) C60, (b) C100, (c) C180, (d) C240.

$$\langle R(t) \rangle = 0, \quad (2a)$$

$$\langle V(0)R(t) \rangle = 0, \quad (2b)$$

$$R(0) = F(0), \quad (2c)$$

where  $F(0) = M\dot{V}(0)$  is the total force acting on the nanoparticle at the initial time and angular brackets,  $\langle \cdot \rangle$ , denote ensemble average. The relation that  $V(0)$  is uncorrelated with  $R(t)$  (Eq. (2b)) means that there is no feedback between the nanoparticle's motion and the projected force exerted by the molecules of the host fluid. All feedback information or the memory is contained in the memory function  $K(t)$ , which connects the current value of the velocity with its values in the past. Further, the fluctuation-dissipation (FD) theorem provides the relation between the autocorrelation function of the projected force in terms of memory function as<sup>4,5</sup>

$$\langle R(0)R(t) \rangle = \langle P^2 \rangle K(t), \quad (3)$$

where  $\langle P^2 \rangle$  is the mean squared momentum ( $P = MV$ ) of the nanoparticle. The general advantage of the GLE formulation is that the complicated many-body interactions of the particle with the host fluid environment are coarse-grained and entirely described by a time-dependent memory function  $K(t)$ . The form of the memory function chosen in this work represents the interaction of the nanoparticle with the host fluid that is assumed to be in equilibrium. Therefore, the memory of the particle only relates its present dynamics at time  $t$  to a past time  $t'$  by a stationary form of memory kernel  $K(t-t')$  in Eq. (1a). However, for the cases where the host fluid undergoes a non-equilibrium transition to a different macrostate, the choice of a non-stationary memory function  $K(t, t')$  is appropriate.<sup>10,11</sup> Such situations often arise in the context of chemical reactions, or change in the host fluid thermodynamic state or the host fluid response to an external force.<sup>12,13</sup> The practical use of GLE can only be made if we have a means to compute the memory function and assign a statistical model to the projected force. Though Mori's microscopic derivation provides the expressions for the

memory function and the projected force, they are extremely involved and are often difficult to evaluate analytically, except for certain limiting situations. Furthermore, determination of the memory function and extraction of the projected force from MD simulation, in which Hamilton's equations of motion for the entire system are solved numerically, are also not straightforward. The difficulty arises from the fact that the projection dynamics entering the definitions of the memory function and the projected force requires the propagation of the observables instead of configurations.<sup>14</sup> The common approaches used to extract these quantities from MD simulation are either through inversion of the GLE using Laplace transform or through rewriting the GLE as a Volterra type equation, commonly referred to as the memory function equation. Multiplying both sides of Eq. (1a) by  $MV(0)$ , and performing the ensemble average using the statistical properties of the projected force (Eq. (2b)), one obtains a memory function equation for the momentum autocorrelation function  $C(t) = \langle P(0)P(t) \rangle$  in terms of  $K(t)$  as

$$\dot{C}(t) = - \int_0^t K(t-s)C(s)ds. \quad (4)$$

The momentum autocorrelation function  $C(t)$  is an observable that is easily computed from the MD simulation, and then Eq. (4) is inverted numerically to obtain the memory function  $K(t)$ . Similarly, using Laplace transform, a closed form equation for the autocorrelation of the projected force can be written in terms of the autocorrelation function of the total force as<sup>15</sup>

$$\langle R(0)R(s) \rangle = \langle F(0)F(s) \rangle \left[ 1 - \frac{\langle F(0)F(s) \rangle}{s\langle P^2 \rangle} \right]^{-1}, \quad (5)$$

where  $s$  is the Laplace variable and  $\langle R(0)R(s) \rangle$ ,  $\langle F(0)F(s) \rangle$  are, respectively, the Laplace transform of the projected and the total force autocorrelation. Also, once the memory function is known, the FD relation (Eq. (3)) can be used to estimate the autocorrelation of the projected force. Higher order correlation functions of the projected force and consequently higher than second moments of the relevant GLE variables ( $X$  and  $V$ ) remain unspecified within Mori's theory. The detailed microscopic derivation of the GLE and the corresponding microscopic expressions for the projected force and the memory function can be found in Refs. 4, 5, 16, and 17.

Before we study the memory function of nanoparticles, we discuss the generalized equipartition theorem for finite-size MD ensembles with PBCs. The generalized equipartition theorem is utilized to compute the mean squared momentum  $\langle P^2 \rangle$  of the nanoparticle. In MD simulations, PBC are typically applied to mimic the behavior of the bulk fluids. When PBCs are applied during equilibrium MD simulations, the total linear momentum is maintained equal to zero to prevent the drifting of the center of mass of the system. Due to this total linear momentum conservation constraint, the momentum of one of the particles is no longer independent of the momenta of the remaining particles, and the usual unconstrained result of  $\langle P^2 \rangle = dMk_B T$  ( $d$  is the system dimensionality,  $k_B$  is the Boltzmann constant, and  $T$  is the temperature of the host-fluid environment) gets modified. This modification can be significant in magnitude if there are unequal mass particles

in the system. In a canonical or NVT ensemble with the constraint that the total linear momentum of the system is zero, the mean squared momentum of the nanoparticle is given by<sup>18,19</sup>

$$\langle P^2 \rangle = 2M \left( 1 - \frac{M}{M_{Total}} \right) \frac{dk_B T}{2} \equiv \mu dk_B T, \quad (6)$$

where  $M_{Total} = M + Nm$  is the total mass and  $\mu = M(1 - M/M_{Total})$  is the reduced mass of the system. The imposition of the zero total linear momentum constraint reduces the mean squared momentum of the nanoparticle by an amount equal to  $M/M_{Total}$ , a factor which depends both on the mass  $M$  of the nanoparticle and the size  $N$  of the system. For identical mass particles ( $M = m$ ,  $M/M_{Total} = 1/N + 1$ ), the reduction is negligible (less than 1% for  $N > 100$ ). However, for unequal mass particles, this reduction can be quite large, especially when  $M \gg m$ . Similarly, in a microcanonical or NVE ensemble, the additional constraint of zero total linear momentum modifies the mean squared momentum as<sup>15,18,19</sup>

$$\langle P^2 \rangle = 2M \left( 1 - \frac{M}{M_{Total}} \right) \frac{\langle E - U \rangle}{N} \equiv 2\mu \frac{\langle E - U \rangle}{N}, \quad (7)$$

where  $E$  is the total energy,  $U$  is the potential energy, and  $\langle E - U \rangle$  is the average kinetic energy of the system. If we replace  $\langle E - U \rangle = dNk_B T/2$ , we see that the canonical distribution result given by Eq. (6) is obtained. These results will be used to both assess the accuracy of MD simulations and understand the scaling of the memory function with the mass of the nanoparticle.

### III. SIMULATION DETAILS

MD simulations are performed using LAMMPS.<sup>20</sup> Each fullerene molecule is modeled as a rigid body using the fix “rigid/NVE” in LAMMPS, which integrates the equation of motion such that the body moves and rotates as a single entity. Simple point charge-extended (SPC/E)<sup>21</sup> model is used for water. Particle-Particle Particle-Mesh (PPPM) method is used to compute the long range electrostatic interactions. To model water-fullerene non-bonded interactions, we use the water-carbon interaction parameters proposed recently by Wu and Aluru.<sup>22</sup> These parameters are developed entirely from *ab-initio* calculation data and predict the graphite-water contact angle and water-carbon nanotube radial breathing mode frequency shift in close agreement with experimental results. For equilibrium MD simulations, an initial 2-5 ns equilibration of the nanoparticle-water system is performed in the NVT ensemble with a Nosé–Hoover thermostat.<sup>23</sup> After equilibration, computations are performed in the NVE ensemble. For transport simulations, the external force on the fullerene molecule and the potential barrier are, respectively, defined using the fix “gravity and addforce” and partial thermostat is applied on the water molecules in the non-streaming directions.

The memory function equation (Eq. (4)) is solved numerically using the algorithm discussed by Berne and Harp in Ref. 16. GLE simulation requires generation of zero mean correlated Gaussian random numbers and a time

integration scheme to numerically solve Eqs. (1b) and (1a). We use an approximate frequency domain method to generate a sequence  $\{R\}$  of zero mean Gaussian random numbers with a specified autocorrelation function  $s_R = \langle P^2 \rangle K(t)$ .<sup>24</sup> The method is as follows: First, using the autocorrelation function  $s_R$ , the spectral density  $S_R$  is computed as

$$S_R(f_j) \equiv \sum_{\tau=-\frac{Q}{2}}^{\frac{Q}{2}} s_R e^{-i2\pi f_j \tau}, \quad 0 \leq j \leq \frac{Q}{2}, \quad (8)$$

where  $Q$  is any even positive number (typically a power of 2) greater than or equal to the desired length of the sequence and  $f_j = \frac{j}{Q}$ . Then, using a sequence  $\{W_j\}$ ,  $j = 0, \dots, Q-1$  of  $Q$  independent and identically distributed Gaussian random numbers with zero mean and unit variance, the sequence  $\{R\}$  is generated as

$$R \equiv \frac{1}{\sqrt{Q}} \sum_{j=0}^{Q-1} R_j e^{-i2\pi f_j t}, \quad t = 0, \dots, Q-1, \quad (9)$$

where  $R_j$  is defined as

$$R_j \equiv \begin{cases} \sqrt{S_R(0)}W_0, & j = 0, \\ \sqrt{\frac{1}{2}S_R(f_j)}(W_{2j-1} + iW_{2j}), & 1 \leq j < \frac{Q}{2}, \\ \sqrt{S_R(\frac{1}{2})}W_{Q-1}, & j = \frac{Q}{2}, \\ R_{Q-j}^*, & \frac{Q}{2} < j \leq Q-1. \end{cases} \quad (10)$$

Here asterisk (\*) denotes the complex conjugate. The frequency domain method is computationally faster ( $O(Q \log Q)$ ) than traditional time domain methods such as Cholesky factorization and Levinson-Durbin recursion ( $O(Q^2)$ ).<sup>24</sup> To integrate the GLE in time, we use a modified Verlet algorithm proposed by Berkowitz, Morgan, and McCammon in Ref. 25. We briefly review the algorithm here. The Verlet algorithm<sup>26</sup> updates the position and velocity of a particle of mass  $M$  as

$$X_{n+1} = -X_{n-1} + 2X_n + \frac{F_n}{M} \Delta t^2, \quad (11a)$$

$$V_n = \frac{X_{n+1} - X_{n-1}}{2\Delta t}, \quad (11b)$$

where  $X_n$ ,  $V_n$  and  $F_n$  are, respectively, the position, velocity and total force at step  $n$  ( $n > 0$ ), and  $\Delta t$  is the time step of the integration. In GLE (Eq. (1a)), the total force at time  $t$  is given as

$$F(t) = -M \int_0^t K(t')V(t-t')dt' + R(t). \quad (12)$$

By approximating the integral in Eq. (12) by a quadrature formula such as trapezoidal rule, the total force  $F_n$  at step  $n > 0$  can be computed as

$$F_n = -M\Delta t \sum_{j=0}^n K_j V_{n-j} w_j + R_n, \quad (13a)$$

$$F_n = -M\Delta t K_0 V_n w_0 + \sum_{j=1}^n K_j V_{n-j} w_j + R_n, \quad (13b)$$

where  $K_0 = K(t=0)$ ,  $w_j$  is the weight factor of the integrand at discrete point  $j$  (for trapezoidal rule, the weights  $w_j$  are  $1/2$  for  $j=0, n$  and  $1$  for  $j=1, \dots, n-1$ ), and  $R_n$  is a particular realization of the random force at step  $n$ . Substituting Eq. (13b) in Eq. (11a) and using the expression for  $V_n$  (Eq. (11b)), one obtains an expression for the position at  $n+1$  step as

$$X_{n+1} \left[ 1 + K_0 \Delta t^2 w_0 / 2 \right] = -X_{n-1} \left[ 1 - K_0 \Delta t^2 w_0 / 2 \right] + 2X_n - \Delta t^3 \sum_{j=1}^n K_j V_{n-j} w_j + R_n \Delta t^2 / M. \quad (14)$$

To use Eq. (14),  $X_0$  and  $X_1$  are needed. One can choose any value for  $X_0$  and compute  $X_1$  using Eq. (11a) as

$$X_1 = X_0 + V_0 \Delta t + \frac{F_0}{M} \Delta t^2, \quad (15)$$

where  $V_0$  is drawn from a Maxwellian distribution corresponding to temperature  $T$ , and  $F_0 = R(0)$ . Once  $X_1$  is computed, Eqs. (14) and (11b) are used to update the position and the velocity in time. We have used  $\Delta t = 0.01$  ps in our simulations.

## IV. RESULTS

### A. Different mass nanoparticles

In this section, we use the GLE formulation to compute the memory function  $K(t)$  and investigate its scaling with the mass of the nanoparticle. The systems we study are different mass C60 fullerene molecule (Fig. 1(a)) immersed in bulk water ( $m = 18$  amu) at 1 bar pressure and 298 K temperature. The mass  $M$  of the C60 molecule is varied by changing the mass of its constituent carbon atoms by a factor of 1, 10, and 100, corresponding to the mass ratio  $M/m$  of 40, 400, and 4000, respectively. Figure 2(a) shows the center of mass (COM) momentum autocorrelation function,  $C(t)$ , of the C60 molecule for different mass ratios.  $C(t)$  are normalized by their initial values. It can be observed that as the mass ratio is increased, the behavior of  $C(t)$  changes from a non-linear oscillatory type decay to a featureless exponential decay. Once  $C(t)$  is obtained from MD simulation, Eq. (4) is used to compute its memory function  $K(t)$ . Figure 2(b) shows the comparison of the memory function  $K(t)$  for different mass ratios. The first thing to observe is that the initial value  $K(0)$  decreases with the increase in the mass ratio. This can be explained as follows: Eq. (4) can be differentiated with

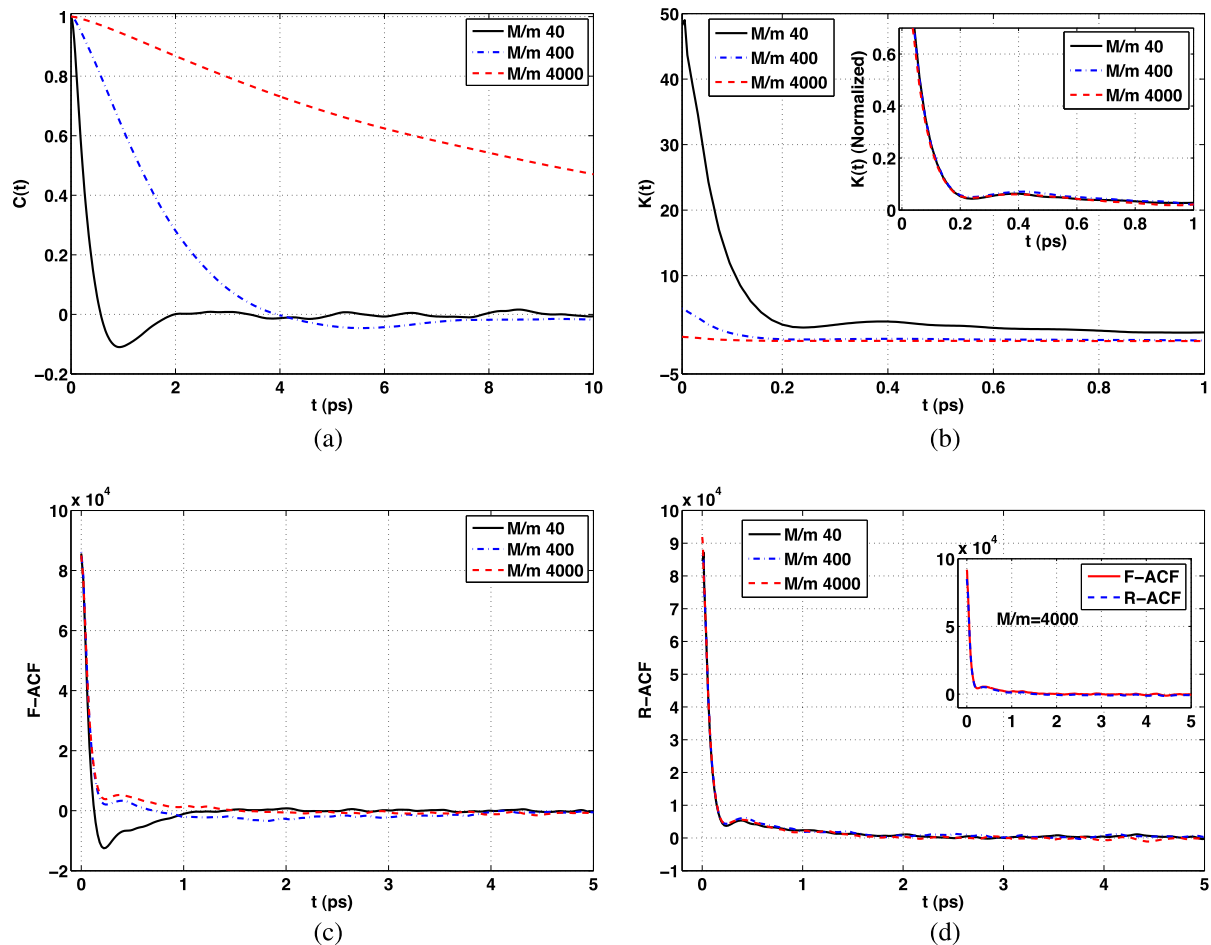


FIG. 2. Comparison of (a) momentum autocorrelation function,  $C(t)$ , (b) memory function,  $K(t)$  (inset: normalized  $K(t)$ ), (c) total force autocorrelation, F-ACF, and (d) projected force autocorrelation, R-ACF (inset: comparison of F-ACF and R-ACF for  $M/m = 4000$ ) for different mass C60 immersed in water.

respect to time to obtain  $K(0)$  as

$$K(0) = -\frac{\dot{C}(0)}{C(0)}. \quad (16)$$

Using the properties of the derivatives of stationary autocorrelation functions, we have  $\dot{C}(0) = -\langle F^2(0) \rangle$ ,<sup>27</sup> where  $\langle F^2(0) \rangle$  is the variance of the total force experienced by the nanoparticle. Figure 2(c) shows the total force autocorrelation function  $F$ -ACF of the C60 molecule for different mass ratios. It can be observed that though the time decay of  $F$ -ACF is different for different mass ratios, the variance  $\langle F^2(0) \rangle$  is almost the same and is independent of the mass of the nanoparticle. This is physically expected as  $\langle F^2(0) \rangle$  only depends on the host-fluid's thermodynamic state and the nature of interaction between the nanoparticle and the host fluid molecules. From the FD relation (Eq. (6)), we know that  $C(0)$  is directly proportional to the reduced mass of the system. Thus,  $K(0)$  is inversely proportional to the reduced mass of the system and decreases with increase in the reduced mass ratio. Now, we compare the functional-form of the memory function. The inset of Fig. 2(d) shows the comparison of the time decay of the normalized memory functions. The memory functions are normalized by their initial values. It can be observed that the time decay of  $K(t)$  is very similar for the three mass ratios. As  $\dot{C}(0)$  does not change with mass, changing the mass of the nanoparticle from  $M$  to  $\tilde{M}$  simply rescales the memory function as

$$\frac{K_{\tilde{M}}(0)}{K_M(0)} = \frac{C_M(0)}{C_{\tilde{M}}(0)}, \quad (17a)$$

$$K_{\tilde{M}}(t) = \frac{\mu_M}{\mu_{\tilde{M}}} K_M(t). \quad (17b)$$

Here symbols with the subscripts  $M$  and  $\tilde{M}$  have their usual meaning as defined above and refer to the quantities associated with the masses  $M$  and  $\tilde{M}$ . We have used the generalized equipartition theorem result (Eq. (6)) in Eq. (17a) to obtain Eq. (17b). Thus, changing the mass of the nanoparticle leads to a simple rescaling of the memory function with the reduced mass of the system. We now show the validity of the generalized equipartition theorem results for a finite-size MD ensemble of unequal mass particles and applied PBC. Table I reports the comparison of the mean squared momentum  $\langle P^2 \rangle$  of the nanoparticle computed using Eq. (7) with the  $C(0)$  value obtained from MD simulation data. It can be observed that the two values are in good agreement with each other. It should be noted that for a mass ratio of 4000 ( $N = 10\,027$ ), the imposition of zero total linear momentum constraint reduces the mean squared momentum of the nanoparticle by  $\sim 30\%$  in comparison to the value of  $\langle P^2 \rangle = 3Mk_B T$ . Once  $C(t)$  and  $K(t)$  are known, a simple measure of the memory can be

defined through a non-dimensional parameter  $\delta$  as<sup>28</sup>

$$\delta = \frac{\tau_C^2}{\tau_K^2}, \quad (18a)$$

$$\tau_C^2 = \left| \int_0^\infty t \tilde{C}(t) dt \right|, \tau_K^2 = \left| \int_0^\infty t \tilde{K}(t) dt \right|, \quad (18b)$$

$$\tilde{C}(t) = \frac{C(t)}{C(0)}, \tilde{K}(t) = \frac{K(t)}{K(0)}, \quad (18c)$$

where  $\tau_C^2$  and  $\tau_K^2$  are the squared characteristic relaxation scales of the momentum autocorrelation function and its memory function, respectively. The limit  $\delta \rightarrow \infty$  corresponds to memoryless behavior ( $\tau_C^2 \gg \tau_K^2$ ) while strong memory effects correspond to the limit  $\delta \rightarrow 0$  ( $\tau_C^2 \ll \tau_K^2$ ). We wish to point out that in long time hydrodynamic limit ( $t \rightarrow \infty$ ), both  $C(t)$  and  $K(t)$  scale as  $t^{-d/2}$ , where  $d$  is the dimensionality of the system.<sup>29,30</sup> In this limit, both time integrals  $\tau_C^2$  and  $\tau_K^2$  diverge. However, the ratio  $\delta$  is guaranteed to converge to zero, reflecting a high measure of hydrodynamic memory in the system.<sup>28</sup> With this understanding, we truncate the integral at short time scales (upper limit changed from  $\infty$  to a cut off time  $t_m \sim 10$  ps) to quantify the degree of the memory in the diffusive regime. The relaxation times and the  $\delta$  values for the three mass ratios are reported in Table I. Since the time decay of the memory function is almost same for all the three mass ratios,  $\tau_K^2$  values are very similar. However,  $\tau_C^2$  increases with increase in the mass ratio and the relaxation process changes from one with strong-memory (smaller  $\delta$  value) for smaller mass ratio to memoryless (bigger  $\delta$  value) for larger mass ratios. This observation can be explained as follows: Since the memory relaxation time remains the same and only its initial value is changed for different mass ratios, we can approximate the memory function as  $K(t) = K(0) \exp(-\lambda t)$ , where  $\lambda$  is the time constant. Now, differentiating Eq. (4) with respect to time, and using  $K(t) = K(0) \exp(-\lambda t)$ , one can obtain an equation for  $\dot{C}(t)$  as

$$\dot{C}(t) = -K(0)C(t) - \int_0^t \dot{K}(t-t')C(t')dt', \quad (19a)$$

$$\dot{K}(t) = -\lambda K(t), \quad (19b)$$

$$\dot{C}(t) + \lambda \dot{C}(t) + K(0)C(t) = 0. \quad (19c)$$

Eq. (19c) is the familiar equation of motion of a damped harmonic oscillator, where  $K(0)$  defines the frequency and  $\lambda$  is the damping constant. As the damping constant  $\lambda$  is the same for all mass ratios, it is essentially  $K(0)$  that determines the behavior of  $C(t)$ . When  $K(0)$  is small ( $K(0) \rightarrow 0$ ), as it is for larger mass ratios,  $C(t)$  exhibits an exponentially decaying behavior with time constant  $\lambda$ , while for larger values of  $K(0)$ ,  $C(t)$  exhibits non-linear oscillatory decay, as observed for smaller mass ratios. We also report in Table I the diffusion

TABLE I. Scaling of memory with the mass of the nanoparticle.

$M/m$	$\langle P^2 \rangle^a$	$C(0)$	$\tau_K^2$ (ps <sup>2</sup> )	$\tau_C^2$ (ps <sup>2</sup> )	$\delta = \tau_C^2/\tau_K^2$	$D \times 10^{-4}$ (nm <sup>2</sup> /ps)
40	$5.34 \times 10^3$	$5.27 \times 10^3$	$0.0853 \pm 0.0061$	$0.1065 \pm 0.0088$	$1.2493 \pm 0.1362$	$4.98 \pm 0.02$
400	$5.15 \times 10^4$	$5.14 \times 10^4$	$0.1072 \pm 0.0150$	$1.4293 \pm 0.0951$	$13.3235 \pm 2.0633$	$4.38 \pm 0.28$
4000	$3.83 \times 10^5$	$3.76 \times 10^5$	$0.0294 \pm 0.0046$	$36.251 \pm 0.2264$	$1232.75 \pm 195.145$	$4.44 \pm 0.48$

<sup>a</sup>Computed using Eq. (7).

coefficient  $D$  of the nanoparticle for the three mass ratios. The diffusion coefficient can be computed from the memory function  $K(t)$  as<sup>17</sup>

$$D = \frac{k_B T}{M} \left[ \int_0^\infty K(t) dt \right]^{-1}. \quad (20)$$

It can be observed that the diffusion coefficient does not change (6% deviation) with the change in the mass of the nanoparticle, which is in accordance with the prediction from the classical Stokes-Einstein relation.<sup>31</sup> For consistency check, we compare in Fig. 2(d), the autocorrelation function of the projected force  $R$ -ACF, which is the force that the host fluid molecules exert on the nanoparticle. It can be observed that it is almost identical for the three mass ratios, which is expected as the projected force does not depend on the mass of the nanoparticle.<sup>4</sup> Also, we show in inset of Fig. 2(d) the comparison of  $F$ -ACF and  $R$ -ACF for the mass ratio 4000. It can be observed that  $F$ -ACF and  $R$ -ACF are very close to each other, thus confirming the assumption that as the Brownian limit<sup>15</sup> is approached ( $M/m \rightarrow \infty$  and  $N \rightarrow \infty$ , giving  $\langle P^2 \rangle \rightarrow \infty$  in Eq. (5)), the autocorrelation of the projected and the total force is identical. However, the true Brownian limit for fixed density particles is given as  $\rho_M/\rho_m \rightarrow \infty$ , where  $\rho_M$  and  $\rho_m$  are nanoparticle and solvent mass densities, respectively.<sup>32,33</sup> Though we report the results for different mass C60 molecule immersed in water,

this global rescaling of the memory function with the reduced mass is observed for other shape and size fullerene molecules considered in this work.

## B. Different shape and size nanoparticles

In this section we investigate the scaling of the memory function with the change in the shape and size of the nanoparticles. We consider C60, C100, C180, and C240 molecules (see Fig. 1) immersed in bulk water at 1 bar pressure and 298 K temperature. For multi-atom clusters like fullerenes, both the arrangement of the constituent atoms and the size influence their dynamics and transport in the host-fluid environment. It has been reported that shape anisotropy and initial orientation of a nanoparticle significantly affect its translocation across biological membranes and are used as controlling factors to design efficient nanoscale drug delivery systems.<sup>9</sup> Also, unlike a smooth spherical particle, the interaction of these multi-atom clusters with the surrounding fluid generates a net torque which gives rise to rotational motion. To understand the memory effects due to shape and size change, we scale the mass of these different shape and size fullerene molecules to maintain a constant mass ratio  $M/m$  of 40. Figures 3(a) and 3(b) show the comparison of the COM  $C(t)$  and  $F$ -ACF, respectively, of different size

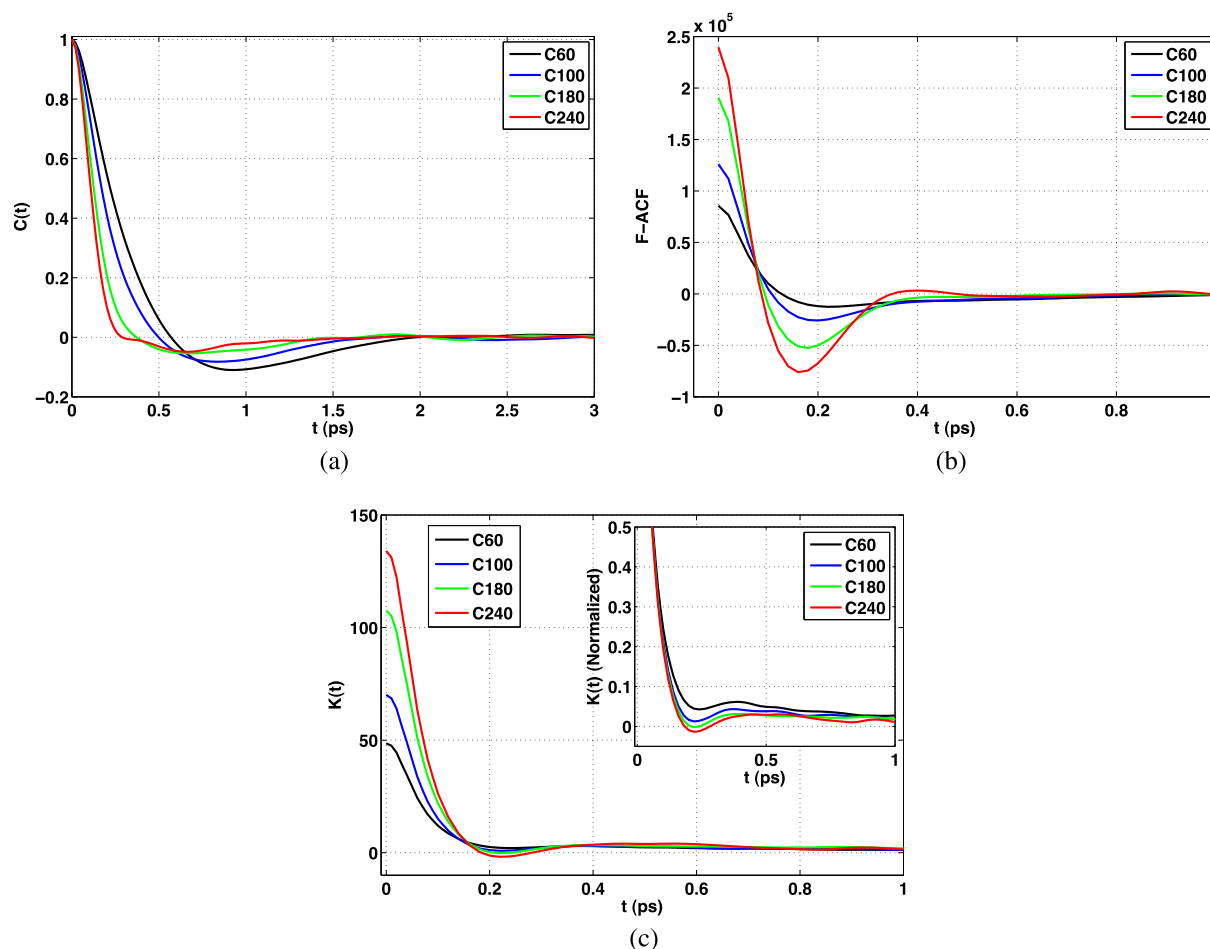


FIG. 3. Comparison of (a) momentum autocorrelation function,  $C(t)$ , (b) total force autocorrelation,  $F$ -ACF, and (c) memory function,  $K(t)$ , for different shape and size nanoparticles ( $M/m = 40$ ) immersed in water.

TABLE II. Scaling of memory with shape and size of the nanoparticle.

Fullerene	$K(0)$ (ps <sup>-2</sup> )	SASA (nm <sup>2</sup> )	$\tau_K^2$ (ps <sup>2</sup> )	$\tau_C^2$ (ps <sup>2</sup> )	$\delta = \tau_C^2/\tau_K^2$	$D \times 10^{-4}$ (nm <sup>2</sup> /ps)
C60	48.75	516.37	0.0853 ± 0.0061	0.1065 ± 0.0088	1.2493 ± 0.1362	4.98 ± 0.02
C100	70.11	697.3	0.0609 ± 0.0110	0.0571 ± 0.0106	0.9364 ± 0.2432	4.32 ± 0.41
C180	107.6	1118.76	0.0394 ± 0.0092	0.0219 ± 0.0095	0.5571 ± 0.2745	3.27 ± 0.37
C240	134.1	1429.26	0.0286 ± 0.0100	0.0344 ± 0.0131	1.2060 ± 0.6243	2.87 ± 0.30

fullerene molecules for  $M/m = 40$ . It can be observed that both  $C(t)$  and  $F$ -ACF show a complicated non-linear behavior for different shape and size molecules. An increased size or solvent accessible surface area (SASA) increases the variance  $\langle F^2(0) \rangle$  of the total force. This is expected as an increased size allows more fluid molecules to interact with the nanoparticle. Fig. 3(c) shows the comparison of the memory function  $K(t)$ . Since the initial value of the memory function is directly proportional to the variance of the total force (Eq. (16)),  $K(0)$  increases with an increase in the size of the nanoparticle. The inset of Fig. 3(c) shows the time decay of the normalized memory function for these molecules. It can be observed that the functional form of the memory function is quite different for different shape and size nanoparticles. Thus, the shape and size of the nanoparticle influence both the initial value and the functional form of the memory function. No simple rescaling relation is observed for the memory functions when the size of the nanoparticle is changed for a fixed mass ratio. Only the initial value  $K(0)$  of the memory function is found to qualitatively scale with the SASA of the fullerene molecules, as observed from Table II. We also report the momentum and the memory relaxation times and the  $\delta$  values for these fullerene molecules. It can be observed that the momentum and memory relaxation times are of comparable magnitude and all these different shape and size nanoparticles exhibit strong memory effects at the mass ratio of 40. Also, from the  $\delta$  values it can be inferred that for a fixed mass ratio, the memory effects are relatively enhanced with the increase in the size of the nanoparticle. We also report in Table II the diffusion coefficient  $D$  of these different shape molecules. It can be observed that  $D$  decreases with increase in the size of the nanoparticle. We also studied the dynamics of these different shape and size fullerene molecules at the mass ratio of 400 and similar conclusions were obtained.

### C. GLE simulation

In this section, we use GLE simulations to investigate the role of memory in nanoparticle dynamics and transport. To highlight the role of memory, we compare the results obtained from GLE simulations with those obtained from static-Langevin equation (SLE), which is extensively used in conjunction with MD to simulate the long time scale behavior of ions/nanoparticles in biological systems.<sup>1-3,34</sup> The SLE is obtained by substituting the memory function  $K(t)$  by  $\gamma\delta(t)$  in Eq. (1a), where  $\gamma = \int_0^\infty K(t)dt$  is a time-independent friction coefficient and  $\delta(t)$  is the Dirac-delta function. The Markovian or “memoryless” property of the projected force in the SLE can be seen through the FD relation (Eq. (3)), which becomes  $\langle R(0)R(t) \rangle = \langle P^2 \rangle \gamma \delta(t)$  when  $K(t) = \gamma \delta(t)$ .

A consequence of the Markovian assumption is that the momentum autocorrelation of the nanoparticle exhibits an exponential decay with time constant  $\gamma^{-1}$ . However, the momentum autocorrelation of fullerenes such as C60 in water exhibits non-exponential decay and contains strong memory effects. As pointed out earlier, the practical use of GLE requires knowing the memory function  $K(t)$  and assigning a statistical model to the projected force  $R(t)$ . A standard choice for  $R(t)$  is to assume that it is Gaussian distributed. There are some studies<sup>35-37</sup> where MD simulation is used to study the statistical properties of the projected force in fluidic systems. All the studies report that for both bulk and confined fluids, the distribution of the projected force is not strictly Gaussian. However, using a Gaussian model for the projected force in the GLE simulations is found to reproduce several important single-particle properties of both bulk and confined fluids in good agreement with MD simulation results.<sup>37,38</sup> So, we assume a zero mean correlated Gaussian model for the projected force, with correlation defined through the FD relation (Eq. (3)). Thus, once the memory function  $K(t)$  is known, GLE can be used to simulate the dynamics and transport of nanoparticles in the host-fluid environment. Here, we want to point out that though the projected force is assumed to be Gaussian, it is still non-Markovian. Doob’s theorem<sup>39</sup> states that a correlated Gaussian process is Markovian if and only if its correlation function is a single exponential. Thus, the trajectories generated from GLE using an arbitrary memory function are in-general non-Markovian. The numerical procedure to solve GLE is discussed in Sec. III. Numerical solution of the SLE requires a trivial modification of the Verlet algorithm discussed in Sec. III and is discussed in Ref. 38.

We first use the GLE simulation to demonstrate the scaling of the memory effects with the change in the initial value of the memory function. We consider two memory functions with different initial values. The first memory function  $K(t)$  is that of the C60 fullerene molecule immersed in bulk water and the second is obtained by scaling  $K(t)$  by a factor of 1/10. This scaling only reduces the magnitude of the second memory function and its correlation time ( $\tau_K^2$ ) is exactly the same as that of the first memory function. The mass  $M$  of the nanoparticle is 720.16 amu. Figure 4(a) shows the comparison of the normalized momentum autocorrelation function  $C(t)$  as obtained from the GLE simulation for these two memory functions. The first observation to be made is that using the memory function for C60, and assuming a Gaussian distribution for the projected force, GLE simulation reproduces the momentum autocorrelation function  $C(t)$  (solid line) in excellent agreement with that obtained from MD simulation (open circle). Second, it can be observed that

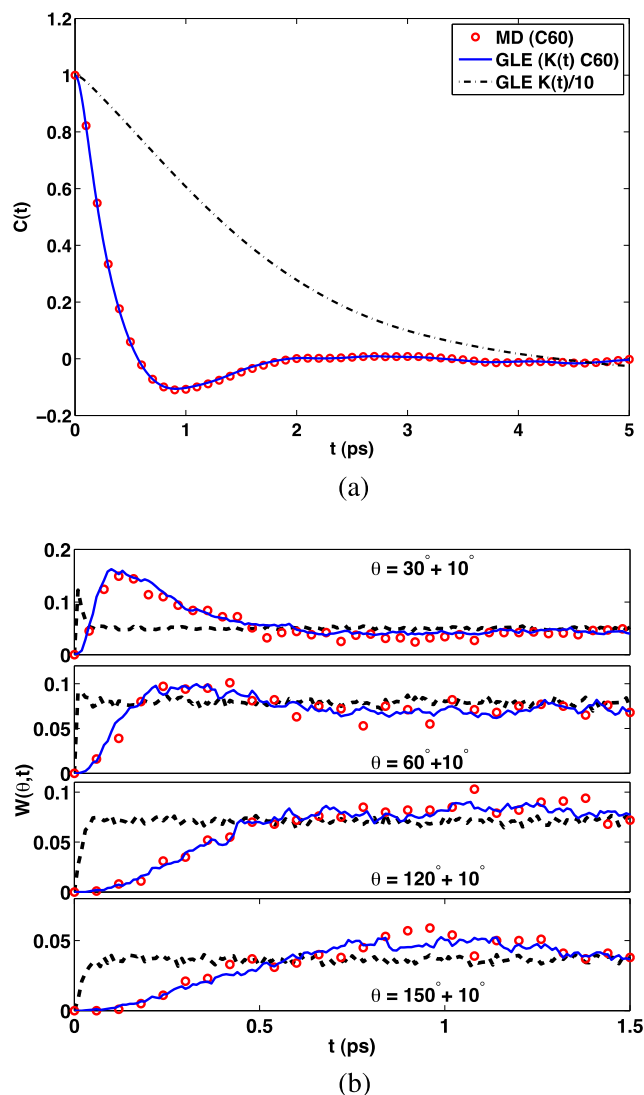


FIG. 4. (a) Scaling of the momentum autocorrelation function with the magnitude of the memory function in GLE simulation, and (b) the time dependence of the probability density  $W(\theta, t)$  for  $\theta = 30^\circ, 60^\circ, 120^\circ$ , and  $150^\circ$ . Solid line is GLE, broken line is SLE, and open circle is MD simulation result.

rescaling the memory function changes the behavior of  $C(t)$  from a non-linear oscillatory type decay to an exponential type decay, thus exhibiting the above observed transition from a strong-memory to a memoryless behavior with the decrease in the initial value of the memory function. Since the momentum autocorrelation function  $C(t)$  is an ensemble averaged quantity, it does not give a very detailed information about the effect of memory on the microscopic motion of the nanoparticle, we study the probability distribution  $W(\theta, t)$  of the angle  $\theta$  formed by the velocity  $V(t)$  of the nanoparticle at time  $t$  with its velocity at an initial time  $V(0)$ ,

$$\theta(t) = \cos^{-1} \left[ \frac{V(0) \cdot V(t)}{\|V(0)\| \|V(t)\|} \right]. \quad (21)$$

Here  $\|V\|$  is the magnitude of the vector  $V$ . The distribution  $W(\theta, t)\Delta\theta$  defines the probability that the angle between the velocity vectors  $V(0)$  and  $V(t)$  is in the interval  $\theta + \Delta\theta$

at time  $t$ .<sup>40,41</sup>  $\theta$  in the range  $0^\circ < \theta < 90^\circ$  signifies the forward direction motion, while  $90^\circ < \theta < 180^\circ$  indicates the backward direction motion with respect to  $V(0)$  ( $W(\theta, t = 0) = 0$ ). Figure 4(b) shows the time dependence of  $W(\theta, t)$  for a C60 molecule immersed in water at four different  $\theta$  values ( $30^\circ, 60^\circ, 120^\circ, 150^\circ, \Delta\theta = 10^\circ$ ) as obtained from GLE (solid line), SLE (broken line), and MD (open circle) simulations. MD simulation results are used as a benchmark to check the accuracy of the trajectories generated by the GLE simulation, while SLE simulation is used to highlight the discrepancies that can occur when memory effects are neglected. It can be observed from Fig. 4(b) that the presence of memory gives rise to a preferred direction ( $\theta$  value) at different times. At short times (until  $t \sim 0.5$  ps),  $\theta < 90^\circ$  values are the preferred direction, giving rise to a correlated motion in the forward direction. At intermediate times ( $t \sim 0.5$ - $1.5$  ps),  $\theta > 90^\circ$  directions start to build up giving rise to a correlated backward motion. It is only at longer times ( $t > 1.5$  ps) that  $W(\theta, t)$  becomes flat signifying a loss of memory with respect to the initial velocity  $V(0)$ . This correlated forward and backward direction motion can give rise to interesting dynamical and transport behavior in nanofluidic applications. SLE simulation trajectories, which assume that there is no memory associated with the molecular motion, completely fail to reproduce this behavior. The time variation of  $W(\theta, t)$  obtained from SLE trajectories is a featureless flat line giving a near uniform distribution at all the times. The presence of a cusp at small times in the SLE data is a numerical artifact due to the finite time step used to generate the  $\delta$ -correlated noise. It is only at longer times ( $t > 1.5$  ps) that time variation of  $W(\theta, t)$  from GLE, SLE, and MD simulations converges to the same value. It is remarkable to observe that the GLE simulation trajectories reproduce the time dependence of  $W(\theta, t)$  for different  $\theta$  values in very good agreement with MD simulation results. We want to point out that this is a non-trivial result and is one of the most critical tests of the accuracy of the GLE simulation. This is because unlike the momentum autocorrelation function or mean-square-displacement (MSD), which are computed by averaging over several trajectories (ensemble average),  $W(\theta, t)$  is calculated from the time evolution of a single trajectory. This exercise demonstrates that GLE can be used as a reliable stochastic simulation tool to generate microscopic trajectories of a nanoparticle in the host-fluid environment.

Now, we discuss a simple barrier crossing example to highlight the effect this memory-induced forward and backward motion can have on nanoparticle transport. Using GLE and SLE we simulate the transport of C60 through a one-dimensional (1D) Gaussian potential energy barrier  $U$  defined as

$$U = U_0 \exp(-X^2/2b^2), \quad (22)$$

where  $U_0$  is the barrier height and  $b$  is its width. Such Gaussian energy barriers are used as basis functions to model the potential of mean force (PMF) for studying the transport of fullerene-like nanoparticles across lipid bilayers and ion channels.<sup>2,3,34</sup> We compute the average barrier crossing time of a C60 molecule through the barrier, when it is immersed in water and is acted upon by a constant external force  $F_{ext} = Ma$ , where  $a$  is the applied acceleration. A schematic

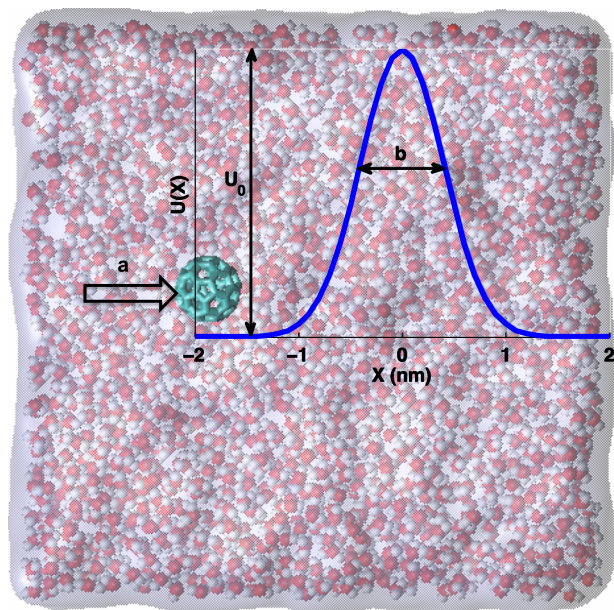


FIG. 5. Schematic of the transport of C60 immersed in water across a 1-D potential barrier  $U(X)$ .

of the system is shown in Fig. 5. Barrier crossing time is defined as the time of transport of the nanoparticle from an initial position  $X(t=0)$  on the left of the barrier to the center of the barrier ( $X=0$ ). Before we discuss the effect of memory on the barrier crossing time, we first show that the steady-state velocity attained by the C60 molecule in the bulk water under the application of a constant external force  $F_{ext}$  (no potential barrier,  $U=0$ ) is the same from both GLE and SLE simulation. Table III shows the comparison of the steady-state velocity of the C60 molecule for the applied acceleration  $a$  of  $0.01 \text{ nm/ps}^2$  as obtained from GLE, SLE, and MD simulation. It can be observed that the steady-state velocities obtained from GLE and SLE simulation are the same and match well with the value obtained from the all-atom MD simulation. It is physically expected because within the linear response regime, the steady state velocity is given by the expression  $F_{ext}/\gamma$ , which is by construction same in both GLE and SLE simulations. Thus, the memory induced forward/backward motion does not alter the long-time steady-state velocity. It only affects the short-time transient motion that characterizes the response or the resistance offered to the C60 molecule by the surrounding water molecules. This short time memory induced transient motion could be significant when studying the transport of the nanoparticle across potential barriers. Table III also reports the average barrier crossing time of a C60 molecule as obtained from GLE, SLE, and MD simulations for the barrier potential parameters of  $U_0 = 2k_B T$ ,  $b = 0.4 \text{ nm}$ ,

TABLE III. Effect of memory on transport properties of the nanoparticle.

	GLE	SLE	MD
Steady-state velocity <sup>a</sup> (nm/ps)	0.0015	0.0014	0.0014
Barrier crossing time <sup>b</sup> (ps)	1299 ( $\pm 565$ )	2599 ( $\pm 323$ )	1580 ( $\pm 798$ )

<sup>a</sup>Parameter:  $a = 0.01 \text{ nm/ps}^2$ .

<sup>b</sup>Parameters:  $U_0 = 2k_B T$ ,  $b = 0.4 \text{ nm}$  and  $a = 0.01 \text{ nm/ps}^2$ .

$a = 0.01 \text{ nm/ps}^2$ . For GLE and SLE simulations, the average barrier crossing time is calculated from the average of 20 simulations, where each simulation is run for 10 ns. MD simulation result is obtained from 5 simulations, where each simulation is run for 9 ns. It can be observed that the average barrier crossing time predicted from SLE is much higher ( $>1 \text{ ns}$ ) than that obtained from GLE simulation. Also, the average barrier crossing time obtained from all-atom MD simulation is much closer to the GLE simulation result. The inclusion of the memory allows the nanoparticle to cross the barrier in lesser time and increases its probability of barrier crossing. This phenomenon of increased probability of barrier crossing with the inclusion of memory is also reported in transport of ions through biological pores.<sup>34</sup> Alternative approaches to decrease the barrier crossing time have also been discussed in the context of modulating the host fluid to a non-equilibrium state,<sup>42</sup> or subjecting the nanoparticle to an external noise source of additive or multiplicative nature.<sup>43,44</sup> Thus, memory effects are important and should be included in the stochastic-simulation based multi-scale approaches used to study the dynamics and transport of fullerene-like nanoparticles in aqueous solution/biological environment.

## V. CONCLUSIONS

Using the GLE formulation, we studied the scaling of the memory function with the mass, shape, and size of fullerene nanoparticles immersed in water. It is observed that changing the mass of the nanoparticle leads to a rescaling of the memory function with the reduced mass of the system. We showed that for different mass nanoparticles it is the initial value of the memory function and not its relaxation time that determines the memory or memoryless behavior. The change in size and the shape of the nanoparticle affects both the functional form and the initial value of the memory function. Using GLE simulations we showed that the memory effects lead to a correlated backward and forward motion which can significantly alter the barrier crossing time of the nanoparticle in host fluid environment.

## ACKNOWLEDGMENTS

This work was supported by the AFOSR under Grant No. FA9550-12-1-0464 and by NSF under Grant Nos. 1264282, 1420882, 1506619, and 1545907. The authors acknowledge the use of the Taub cluster provided by the Computational Science and Engineering Program at the University of Illinois.

<sup>1</sup>O. F. Lange and H. Grubmüller, *J. Chem. Phys.* **124**, 214903 (2006).

<sup>2</sup>D. Gordon, V. Krishnamurthy, and S.-H. Chung, *J. Chem. Phys.* **131**, 134102 (2009).

<sup>3</sup>D. I. Kopelevich, *J. Chem. Phys.* **139**, 134906 (2013).

<sup>4</sup>H. Mori, *Prog. Theor. Phys.* **33**, 423 (1965).

<sup>5</sup>R. Kubo, *Rep. Prog. Phys.* **29**, 255 (1966).

<sup>6</sup>M. S. Dresselhaus, G. Dresselhaus, and P. C. Eklund, *Science of Fullerenes and Carbon Nanotubes: Their Properties and Applications* (Academic Press, 1996).

<sup>7</sup>J. Wong-Ekkabut, S. Baoukina, W. Triampo, I.-M. Tang, D. P. Tieleman, and L. Monticelli, *Nat. Nanotechnol.* **3**, 363 (2008).

<sup>8</sup>R. Maeda-Mamiya, E. Noiri, H. Isobe, W. Nakanishi, K. Okamoto, K. Doi, T. Sugaya, T. Izumi, T. Homma, and E. Nakamura, *Proc. Natl. Acad. Sci. U. S. A.* **107**, 5339 (2010).

- <sup>9</sup>K. Yang and Y.-Q. Ma, *Nat. Nanotechnol.* **5**, 579 (2010).
- <sup>10</sup>S. Kawai and T. Komatsuzaki, *J. Chem. Phys.* **134**, 114523 (2011).
- <sup>11</sup>R. Hernandez and F. L. Somer, *J. Phys. Chem. B* **103**, 1064 (1999).
- <sup>12</sup>A. V. Popov, J. Melvin, and R. Hernandez, *J. Phys. Chem. A* **110**, 1635 (2006).
- <sup>13</sup>A. V. Popov and R. Hernandez, *Phys. Rev. E* **88**, 032145 (2013).
- <sup>14</sup>A. Carof, R. Vuilleumier, and B. Rotenberg, *J. Chem. Phys.* **140**, 124103 (2014).
- <sup>15</sup>P. Español and I. Zuniga, *J. Chem. Phys.* **98**, 574 (1993).
- <sup>16</sup>B. J. Berne and G. D. Harp, *Advances in Chemical Physics* (John Wiley and Sons, Inc., 1970), Vol. 17, pp. 102–106, 217–222.
- <sup>17</sup>J. P. Boon and S. Yip, *Molecular Hydrodynamics* (McGraw-Hill Inc., 1980).
- <sup>18</sup>R. B. Shirts, S. R. Burt, and A. M. Johnson, *J. Chem. Phys.* **125**, 164102 (2006).
- <sup>19</sup>M. J. Uline, D. W. Siderius, and D. S. Corti, *J. Chem. Phys.* **128**, 124301 (2008).
- <sup>20</sup>S. Plimpton, *J. Comput. Phys.* **117**, 1 (1995).
- <sup>21</sup>H. J. C. Berendsen, J. R. Grigera, and T. P. Straatsma, *J. Phys. Chem.* **91**, 6269 (1987).
- <sup>22</sup>Y. Wu and N. Aluru, *J. Phys. Chem. B* **117**, 8802 (2013).
- <sup>23</sup>S. Nosé, *J. Chem. Phys.* **81**, 511 (1984).
- <sup>24</sup>D. B. Percival, *Comput. Sci. Stat.* **24**, 534 (1992).
- <sup>25</sup>M. Berkowitz, J. Morgan, and J. A. McCammon, *J. Chem. Phys.* **78**, 3256 (1983).
- <sup>26</sup>L. Verlet, *Phys. Rev.* **159**, 98 (1967).
- <sup>27</sup>J. S. Bendat and A. G. Piersol, *Random Data: Analysis and Measurement Procedures*, 4th ed. (John Wiley and Sons, Inc., 2010), pp. 109–171.
- <sup>28</sup>A. V. Mokshin, R. M. Yulmetyev, and P. Hänggi, *Phys. Rev. Lett.* **95**, 200601 (2005).
- <sup>29</sup>D. Lesnicki, R. Vuilleumier, A. Carof, and B. Rotenberg, *Phys. Rev. Lett.* **116**, 147804 (2016).
- <sup>30</sup>N. Corngold, *Phys. Rev. A* **6**, 1570 (1972).
- <sup>31</sup>G. K. Batchelor, *An Introduction to Fluid Dynamics* (Cambridge University Press, 2000).
- <sup>32</sup>L. Bocquet, J.-P. Hansen, and J. Piasecki, *J. Stat. Phys.* **76**, 527 (1994).
- <sup>33</sup>L. Bocquet, *Acta Phys. Pol. Ser. B* **29**, 1551 (1998).
- <sup>34</sup>T. Baştuğ and S. Kuyucak, *Chem. Phys. Lett.* **401**, 175 (2005).
- <sup>35</sup>G. Sese, E. Guardia, and J. A. Padro, *J. Stat. Phys.* **60**, 501 (1990).
- <sup>36</sup>H. K. Shin, C. Kim, P. Talkner, and E. K. Lee, *Chem. Phys.* **375**, 316 (2010).
- <sup>37</sup>T. Sanghi and N. Aluru, *J. Chem. Phys.* **141**, 174707 (2014).
- <sup>38</sup>T. Sanghi and N. R. Aluru, *J. Chem. Phys.* **138**, 124109 (2013).
- <sup>39</sup>R. F. Fox, *J. Math. Phys.* **18**, 2331 (1977).
- <sup>40</sup>R. Lynden-Bell, D. Hutchinson, and M. Doyle, *Mol. Phys.* **58**, 307 (1986).
- <sup>41</sup>M. Canales and J. Padró, *Mol. Simul.* **1**, 403 (1988).
- <sup>42</sup>J. R. Chaudhuri, S. K. Banik, S. Chattopadhyay, and P. Chaudhury, *J. Math. Phys.* **49**, 113303 (2008).
- <sup>43</sup>J. R. Chaudhuri, S. Chattopadhyay, and S. K. Banik, *Phys. Rev. E* **76**, 021125 (2007).
- <sup>44</sup>J. R. Chaudhuri, S. Chattopadhyay, and S. K. Banik, *J. Chem. Phys.* **128**, 154513 (2008).